Mathematics and Computers in Simulation 251 (2027) 327–344

Contents lists available at ScienceDirect

Mathematics and Computers in Simulation

journal homepage: www.elsevier.com/locate/matcom

Original articles

Harvesting water in a cyclone chimney designed by means of meta-optimization based on sustainability criteria☆

P. González-Rodelas [a], G. Klochok [b], E. Moreno [c,*]

[a] Departamento de Matemática Aplicada, E.T.S. de Ingeniería de Caminos, Canales y Puertos, Campus Universitario de Fuentenueva (Edificio Politécnico), Granada, 18071, Spain

[b] Moscow State University of Civil Engineering, National Research University, Yaroslavskoye Shosse, Moscow, Russia

[c] CEMDATIC-E.T.S.I Telecommunication and Department of Structures and Building Physics, Escuela Técnica Superior de Arquitectura de Madrid (UPM), Av. de Juan de Herrera, 4, Moncloa-Aravaca, Madrid, 28040, Spain

ARTICLE INFO

Keywords:
Atmospheric water harvesting
Cyclone condensation tower
Passive water harvesting
Reduced-order model
Meta-optimization
Sustainable design

ABSTRACT

This study presents a novel design and optimization approach for atmospheric water condensation towers, leveraging passive cyclonic processes within kinematic chimneys to harvest atmospheric moisture. Aimed at addressing water scarcity in arid regions, the proposed cyclone chimney design is optimized through meta-optimization techniques that prioritize sustainability. The tower system employs a reduced-order model, utilizing eigenfunctions to enhance computational efficiency without sacrificing predictive accuracy, allowing for rapid optimization across diverse environmental and structural parameters. The tower's design incorporates considerations for environmental and economic sustainability, favoring simple durable materials to limit environmental impact and reduce resource costs. The dual deployment capability in agricultural and urban settings highlights the system's adaptability, fostering integrated solutions for resource management. Simulation results indicate that the system can achieve an average daily water yield of 57 liters, with performance adjusted for seasonal variations. The design's minimal energy requirements and modular structure demonstrate its suitability for implementation in regions with high water demand and limited resources. This study advances sustainable water harvesting technology by aligning technical, environmental, and social goals, with the potential for broader applications in climates affected by water scarcity.

1. Introduction

Freshwater scarcity is emerging as one of the defining constraints of the twenty-first century. Water stress is no longer a localized phenomenon restricted to arid regions, but a systemic condition driven by climate change, population growth, agricultural demand, and the degradation of natural water sources. Recent global assessments indicate that a significant fraction of the world's population experiences severe water scarcity during at least part of the year [1]. Consequently, water must be understood not only as a natural resource but as a strategic asset with profound socio-economic and geopolitical implications.

This challenge must also be framed within the broader context of material and energetic limits. Modern water production technologies — such as desalination, refrigeration-based condensation, or membrane filtration — depend heavily on energy consumption and material resources. As emphasized in *Thanatia* [2,3], technological systems cannot be decoupled from the depletion

☆ This article is part of a Special issue entitled: 'MATCOM_MACMAS 2025' published in Mathematics and Computers in Simulation.

* Corresponding author.
E-mail address: em.moreno@upm.es (E. Moreno).

https://doi.org/10.1016/j.matcom.2026.07.037
Received 27 November 2025; Received in revised form 17 July 2026; Accepted 26 July 2026
Available online 1 August 2026
0378-4754/© 2026 The Authors. Published by Elsevier B.V. on behalf of International Association for Mathematics and Computers in Simulation (IMACS). This is an open access article under the CC BY-NC-ND license (http://creativecommons.org/licenses/by-nc-nd/4.0/).

and degradation of mineral resources, imposing thermodynamic and ecological constraints on large-scale solutions. Therefore, the key question is not only how to produce water, but how to do so within the limits of resource availability and long-term sustainability.

Within this context, atmospheric water harvesting (AWH) has emerged as a promising alternative, treating atmospheric humidity as a distributed and renewable reservoir. Existing technologies can be broadly classified into condensation-based systems, sorption-based systems, and hybrid approaches [4]. Condensation systems, such as vapor-compression cycles, are mature and capable of relatively high production rates, but require continuous energy input. Sorption-based systems, including those based on metal–organic frameworks (MOFs), enable operation at lower relative humidity levels, but rely on cyclic processes and thermal regeneration, limiting their continuity and efficiency. Hybrid systems attempt to combine advantages from both approaches, but often introduce additional complexity, cost, and material dependency.

A critical analysis of these technologies reveals a common limitation: their reliance on energy input, complex materials, or active components. Metrics such as the Water Harvesting Rate (WHR) and the Unitary Power Consumption (UPC) highlight a fundamental trade-off between production capacity and energy consumption, raising questions regarding scalability and sustainability, particularly in remote or resource-constrained environments.

In contrast, passive systems offer an alternative paradigm. These systems exploit natural gradients of temperature, pressure, and humidity to induce condensation without external mechanical energy input. Among them, cyclone-based condensation towers represent a particularly promising approach. Their conceptual foundations can be traced to solar chimney and cyclone-assisted flow systems [5–11], where buoyancy-driven airflow and pressure differentials are used to enhance evaporation and condensation processes.

The cyclone chimney concept introduces an additional mechanism: rotational flow, which increases residence time and promotes condensation through enhanced mixing and centrifugal effects [7]. However, many of these proposals remain either theoretical or based on large-scale infrastructures, raising concerns regarding feasibility, cost, and environmental impact. Moreover, there exists a gap between conceptual feasibility and practical design optimization under realistic environmental conditions.

The present work addresses this gap by proposing a fully passive cyclone-based tower designed to harvest atmospheric moisture under suitable environmental conditions. The system relies on the interaction between thermal gradients, pressure differences, and controlled airflow to induce continuous condensation without external energy input. A detailed description of the physical operating principles and internal flow mechanisms is provided in Section 2.

Beyond the physical concept, the main contribution of this work is methodological. Rather than focusing solely on a specific configuration, the study develops a general optimization framework that can be applied to this technology and extended to other systems. The approach integrates high-fidelity modeling, reduced-order modeling, and multi-objective optimization within a unified pipeline.

This methodology can be understood as a meta-optimization framework, in which the optimization process itself is preconditioned and structured to improve both efficiency and physical relevance. First, a preliminary stage is introduced to constrain the geometric design space based on economic considerations, identifying configurations that minimize construction cost and defining a feasible region for subsequent analysis.

Second, the high-fidelity model based on coupled partial differential equations is systematically reduced to a lower-dimensional representation, enabling efficient evaluation of system performance within this constrained space.

Third, the discrete temporal solutions obtained from the high-fidelity model—typically evaluated at representative time intervals (e.g., daily conditions)—are mapped onto the reduced-order model and interpolated to construct a continuous temporal response. This extended reduced model allows capturing seasonal variability and enables the prediction of water production over extended time horizons without requiring repeated high-cost simulations.

This multi-layered strategy transforms the original optimization problem into a structured pipeline, where geometry, physics, and temporal variability are consistently integrated, significantly enhancing the tractability and robustness of the design process.

As shown in Fig. 1, the methodology begins with the construction of a high-fidelity numerical model based on a system of coupled partial differential equations. This model accounts for turbulent airflow, heat transfer, and phase change processes, as well as the interaction between the structure and environmental forcing, including wind, solar irradiance, temperature, and relative humidity. The simulations are performed using multiphysics tools such as COMSOL Multiphysics [12], and provide detailed spatial distributions of the relevant physical variables together with reference estimates of water production. Due to the strong coupling between phenomena and the computational complexity of turbulent flow with phase change, this model requires significant computational resources and long simulation times. To overcome these limitations, a reduced-order model is constructed from the high-fidelity simulations using an eigenvalue–eigenfunction decomposition. This reduced model captures the essential dynamics of the system within a defined range of environmental and geometric parameters, enabling rapid evaluation of system performance. The inputs to this model include both environmental variables (temperature, humidity, irradiance, wind conditions) and geometric parameters (height, radius, wall thickness), while the primary output is the amount of water harvested over a given period.

The reduced model serves as the core tool for the optimization stage, which is formulated as a two-step process. First, an economical model is introduced to identify the geometric variables that have the greatest impact on construction cost, allowing the definition of feasible design regions. Second, a multi-objective optimization problem is solved using Karush–Kuhn–Tucker (KKT) conditions [13,14], aiming to maximize water production while minimizing economic cost. This approach can be interpreted as a meta-optimization process, where the trade-off between performance and resource expenditure is explicitly addressed through geometric design.

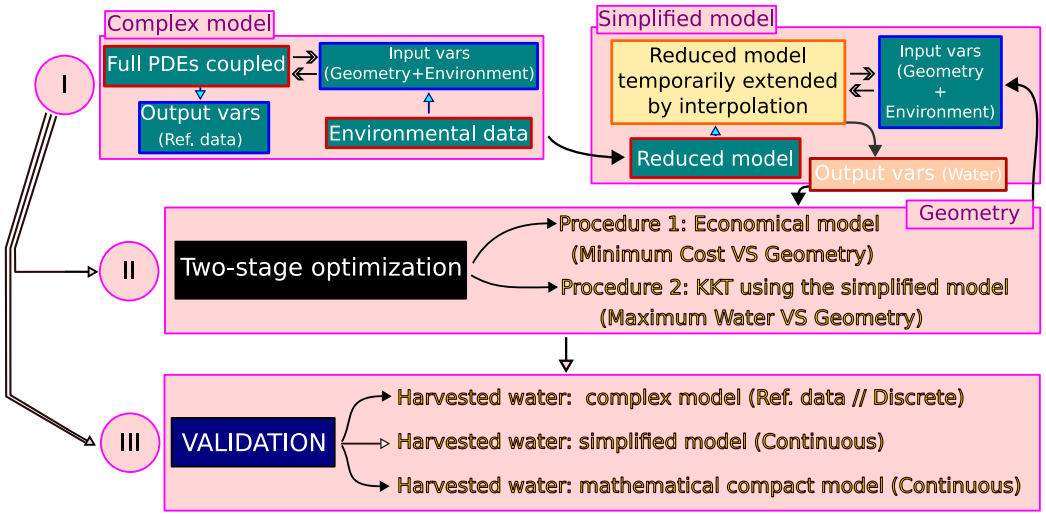


Fig. 1. Schematic representation of the multistage methodology. (I) A high-fidelity model based on fully coupled partial differential equations (PDEs) provides reference data using environmental inputs. A reduced-order model is subsequently derived from this complex model. (II) The reduced-order model is employed in a two-stage optimization process, including an economical model (cost vs. geometry) and a Karush–Kuhn–Tucker (KKT) optimization (water production vs. geometry). (III) Validation is performed by comparing the complex model, the reduced-order model, and a compact mathematical model.

Finally, a validation stage is carried out by comparing the predictions of the reduced model with discrete results obtained from the high-fidelity simulations for selected environmental conditions. In addition, a compact mathematical model is developed, capable of reproducing both the reduced and complex model responses with minimal computational effort. This compact formulation enables rapid estimation of water production as a function of geometry and environmental conditions.

Structure of the paper. The paper is organized as follows. Section 2 presents the physical operating principle of the cyclone condensation tower. Section 3 introduces the high-fidelity multiphysics model together with its reduced-order counterpart for efficient simulations. Section 4 describes the construction of the environmental inputs from meteorological, radiative, and wind data. Section 5 develops the optimization framework, including the cost formulation, global sensitivity analysis, and constrained optimization strategy. Section 6 reports the main numerical results, including water-production estimates and model validation. Finally, Section 7 summarizes the main findings, while additional technical details are provided in the Supplementary Material.

2. Physical principle of operation of the cyclone condensation tower

The proposed system is based on the passive extraction of atmospheric water through the coupling of thermodynamic, fluid dynamic, and geometric effects within a single vertical structure. The operating principle relies on inducing a continuous airflow that undergoes cooling, expansion, and condensation as it traverses the system, driven exclusively by naturally occurring gradients and passive design elements.

2.1. Qualitative description of the process

The overall mechanism is illustrated in Fig. 2, which provides a conceptual representation of the system in three stages. As shown in Fig. 2(a), ambient air is captured through multiple inlets distributed around the structure and guided into underground ducts. These ducts act as thermal stabilizers, exploiting the relatively constant temperature of the ground to cool the incoming air. This mechanism is analogous to earth-air heat exchangers, where the air temperature approaches the ground temperature after sufficient residence time.

The cooling process, depicted in Fig. 2(b), reduces the air temperature while maintaining its absolute humidity. As a result, the relative humidity increases and the air approaches saturation conditions. The geometry of the ducts, including their length and gradual contraction, enhances heat transfer and promotes a controlled flow regime.

Once the air reaches the base of the tower, it is injected tangentially rather than axially. This configuration, shown in Fig. 2(c), induces a cyclonic motion inside the chimney. The resulting helical trajectory increases the residence time of the air and enhances the probability of condensation through prolonged interaction with cooler surfaces.

To further enhance the internal flow dynamics, the system incorporates additional passive design elements. A conical polyethylene pipe located at the top of the tower circulates heated water, typically driven by solar energy in a closed loop. This element introduces a localized thermal gradient, increasing the air temperature in the upper region and consequently reducing its density. The resulting buoyancy effect strengthens the upward airflow and reinforces the chimney-driven circulation.

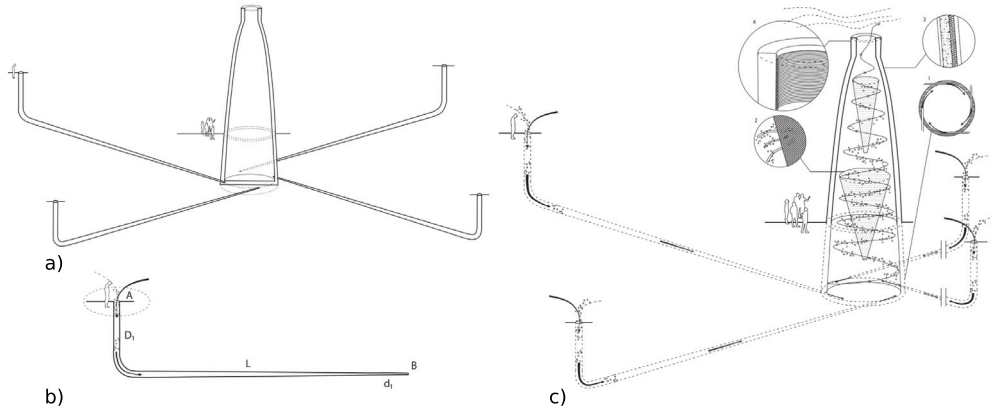


Fig. 2. Qualitative scheme of the cyclone condensation tower. (a) Global configuration of the system showing the underground air intake network and central chimney. (b) Air cooling process through underground ducts. (c) Cyclonic upward motion and condensation inside the tower.

In parallel, the internal geometry of the tower includes flow-guiding structures, here referred to as *trapping profiles*. These elements act as passive aerodynamic deflectors that control the internal flow structure, promoting a stable cyclonic regime and increasing the residence time of humid air. By extending the interaction between the air and the internal surfaces, these profiles enhance heat and mass transfer processes, facilitating condensation and droplet capture without introducing mechanical complexity.

As the air ascends, several coupled mechanisms contribute to further cooling and condensation:

- **Adiabatic expansion**: The reduction in pressure along the vertical axis leads to a decrease in temperature.
- **Convective heat transfer**: Interaction with the tower walls and internal structures facilitates heat exchange.
- **Phase change**: Once the dew point is reached, water vapor condenses on available nucleation surfaces.

Condensed water droplets are transported toward the tower walls by centrifugal forces associated with the cyclonic motion, where they accumulate and are collected through a drainage system. This mechanism ensures continuous water harvesting without requiring external energy input.

2.2. Pressure-driven flow and system self-sustainability

The continuous operation of the system is governed by pressure differences generated by both buoyancy-driven and dynamic effects. A quantitative representation of these mechanisms is shown in Fig. 3. As illustrated in Fig. 3, the pressure at the base of the tower (P_{bottom}) exceeds the pressure at the top (P_{top}), establishing a vertical pressure gradient that drives the airflow:

$$\sum \Delta P = \Delta P_g + \Delta P_{|u|} \tag{1}$$

The pressure difference associated with gravity is more accurately described as a buoyancy-driven (stack effect) contribution, arising from density differences between the air inside and outside the chimney:

$$\Delta P_g = g \int_0^H \left(\rho_{\text{out}}(z) - \rho_{\text{in}}(z)\right) dz \tag{2}$$

Under the assumption of moderate vertical variations, this expression can be approximated as:

$$\Delta P_g \approx gH \left(\rho_{\text{out}} - \rho_{\text{in}}\right) \tag{3}$$

In the present system, the density difference is actively reinforced by the thermal gradient generated at the top of the tower, where the heated pipe reduces the local air density. This effect amplifies buoyancy forces and enhances the upward motion of the flow, inducing a suction mechanism at the base that continuously draws ambient air into the system.

In addition, the cyclonic motion introduces a dynamic pressure contribution associated with the tangential velocity:

$$\Delta P_{|u|} \propto \frac{1}{2}\rho_{\text{air}} u_{\text{tan}}^2 \tag{4}$$

where the tangential velocity is defined as:

$$u_{\text{tan}}^2 = (\vec{u} \cdot \hat{\imath})^2 + (\vec{u} \cdot \hat{\jmath})^2 \tag{5}$$

The combination of buoyancy-driven and velocity-induced effects leads to:

$$P_{\text{bottom}} = P_{\text{top}} + \sum \Delta P \tag{6}$$

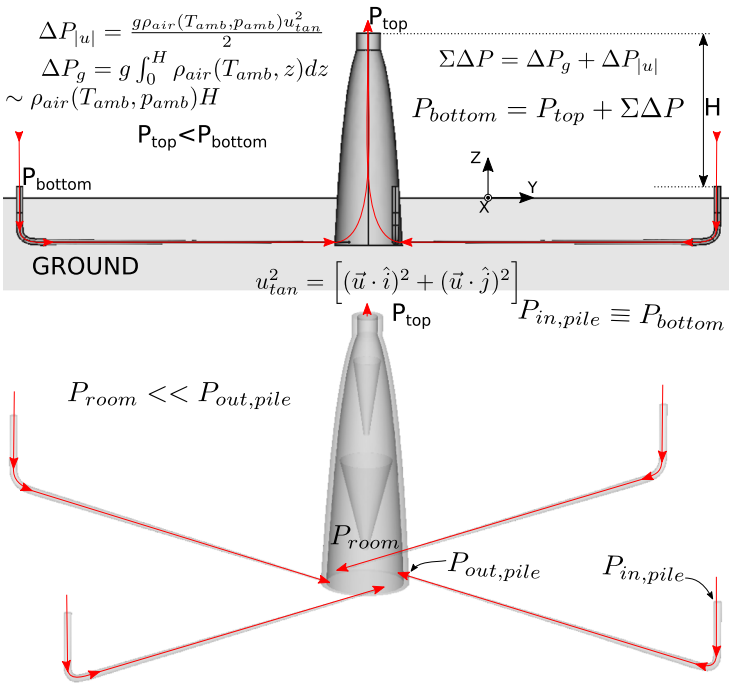


Fig. 3. Quantitative scheme of pressure balance and flow generation. The total pressure difference driving the flow results from the combination of buoyancy-induced and velocity-induced contributions.

ensuring that $P_{bottom} > P_{top}$, which sustains the upward airflow.

An additional key feature of the system is the pressure imbalance between the interior of the tower and the external intake network. As indicated in Fig. 3, the pressure inside the tower (P_{room}) is significantly lower than the pressure at the inlet pipes, promoting continuous air intake:

$$P_{room} \ll P_{out,pile} \approx P_{in,pile} \equiv P_{bottom} \tag{7}$$

This pressure configuration establishes a self-sustained flow loop, where air is continuously drawn into the system, cooled, accelerated, and discharged through the top of the chimney.

2.3. Coupling between geometry, flow, and condensation

The efficiency of the system depends critically on the coupling between geometry, fluid dynamics, and thermodynamics. The height of the tower (H) directly influences the buoyancy-driven pressure gradient, while the inlet configuration determines the magnitude of the tangential velocity and therefore the intensity of the cyclonic motion.

Similarly, the underground duct length and geometry control the pre-conditioning of the air, determining its proximity to saturation before entering the tower. The internal geometry, including the trapping profiles and the tapering of the chimney, governs the flow structure, residence time, and effective heat and mass transfer.

The thermal conditions at the top of the tower, influenced by the heated pipe, further modulate the density field and enhance the driving forces of the system. These coupled effects create a self-regulated configuration in which airflow, cooling, and condensation are intrinsically linked, enabling continuous atmospheric water harvesting without external energy input.

3. Mathematical models

The cyclone condensation tower is governed by the coupled interaction between moist-air flow, turbulence, heat transfer, phase change, and structural response under environmental forcing. In this work, two mathematical descriptions are used: a high-fidelity model, employed to generate reference solutions, and a reduced-order model, used as the computational core of the optimization framework. Detailed derivations, boundary conditions, numerical implementation, mesh settings, and extended simulation results are provided in the Supplementary Material.

3.1. High-fidelity model

The high-fidelity model describes the tower as a coupled multiphysics system solved numerically using COMSOL Multiphysics. The airflow is modeled as turbulent moist air using the Reynolds-averaged Navier–Stokes equations with a k–ε closure. The governing equations for mass and momentum conservation are written as

$$\frac{\partial \rho}{\partial t} + \nabla \cdot (\rho \mathbf{u}) = 0, \tag{8}$$

$$\rho \left(\frac{\partial \mathbf{u}}{\partial t} + (\mathbf{u} \cdot \nabla)\mathbf{u} \right) = \nabla \cdot (-p\mathbf{I} + \mathbf{K}) + \rho \mathbf{g}, \tag{9}$$

where ρ is the moist-air density, $\mathbf{u}$ the velocity field, p the pressure, and $\mathbf{K}$ the effective stress tensor. The turbulent stress contribution is modeled as

$$\mathbf{K} = (\mu + \mu_T) \left[\nabla \mathbf{u} + (\nabla \mathbf{u})^T \right] - \frac{2}{3} \rho k \mathbf{I}, \tag{10}$$

with turbulent viscosity

$$\mu_T = \rho C_\mu \frac{k^2}{\varepsilon}. \tag{11}$$

The transport equations for turbulent kinetic energy k and its dissipation rate ε are

$$\rho \frac{\partial k}{\partial t} + \rho (\mathbf{u} \cdot \nabla) k + \rho \varepsilon = \nabla \cdot \left[\left(\mu + \frac{\mu_T}{\sigma_k} \right) \nabla k \right] + P_k, \tag{12}$$

$$\rho \frac{\partial \varepsilon}{\partial t} + \rho (\mathbf{u} \cdot \nabla) \varepsilon + C_{\varepsilon 2} \rho \frac{\varepsilon^2}{k} = \nabla \cdot \left[\left(\mu + \frac{\mu_T}{\sigma_\varepsilon} \right) \nabla \varepsilon \right] + C_{\varepsilon 1} \frac{\varepsilon}{k} P_k, \tag{13}$$

where

$$P_k = \mu_T \left[\nabla \mathbf{u} : \left(\nabla \mathbf{u} + (\nabla \mathbf{u})^T \right) \right]. \tag{14}$$

The use of a turbulence closure is justified by the local Reynolds number distribution obtained in the tower. Although cyclonic motion does not necessarily imply turbulence — a rotating flow may remain laminar or transitional at sufficiently low velocities — the present configuration develops Reynolds numbers above the conventional turbulent threshold in the main flow regions. As shown in Fig. 4, values larger than $Re \simeq 4000$ are reached in the intake–tower connection and within the lower part of the chimney, where the tangential injection generates the cyclonic core. This supports the use of a RANS formulation with a k–ε closure for the high-fidelity model. The thermal field is governed by an energy balance written in terms of temperature:

$$\rho C_p \left(\frac{\partial T}{\partial t} + \mathbf{u} \cdot \nabla T \right) + \nabla \cdot (\mathbf{q} + \mathbf{q}_R) = \frac{\partial p}{\partial t} + \mathbf{u} \cdot \nabla p + \boldsymbol{\tau} : \nabla \mathbf{u} + Q_H, \tag{15}$$

where T is temperature, C_p is the specific heat capacity, $\mathbf{q}$ is the conductive heat flux, $\mathbf{q}_R$ is the radiative heat flux, $\boldsymbol{\tau} : \nabla \mathbf{u}$ accounts for viscous dissipation, and Q_H represents the enthalpy contribution associated with water-vapor diffusion in moist air.

The moisture content is coupled to the thermal and flow fields through the relative humidity and saturation pressure. Condensation is assumed to occur when the local relative humidity exceeds saturation. The instantaneous water mass flow rate across a collecting section S is computed as

$$\dot{m}_{\mathrm{H_2O}}(t) = \iint_S \left(\rho q_w^{\mathrm{exc}} \right) \mathbf{u} \cdot d\mathbf{S}, \tag{16}$$

where q_w^{exc} is the excess water-vapor mass fraction available for condensation. The corresponding daily harvested volume is

$$V_{\mathrm{H_2O,day}} = \frac{1}{\rho_{\mathrm{H_2O}}} \int_0^{24\ h} \left[\iint_S \left(\rho q_w^{\mathrm{exc}} \right) \mathbf{u} \cdot d\mathbf{S} \right] dt. \tag{17}$$

The high-fidelity model also includes thermal coupling with the solid tower walls and, when required, a structural calculation under wind loading. The mechanical equilibrium of the structure can be expressed as

$$\mathbf{F}_v + \nabla \cdot \mathbf{S} = 0, \tag{18}$$

with aerodynamic loading transferred from the fluid to the structure through

$$\mathbf{F}_a = (-p\mathbf{I} + \mathbf{K}) \cdot \mathbf{n}. \tag{19}$$

This high-fidelity model provides reference solutions for selected environmental and geometric configurations. Because the full problem involves turbulent flow, heat transfer, humidity transport, phase change, and fluid–structure interaction, its computational cost is high. For this reason, it is used only to generate representative solutions and validation data, while the optimization process relies on a reduced-order formulation.

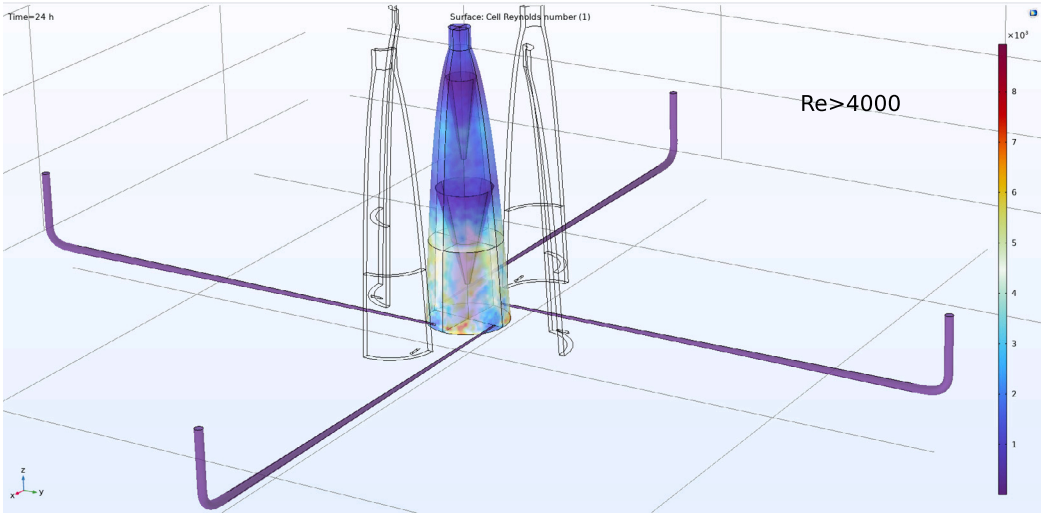


Fig. 4. Local Reynolds number distribution in the cyclone condensation tower. The map shows that the flow reaches values above the conventional turbulent threshold, $Re > 4000$, particularly near the tangential intake region and in the lower part of the chimney, where the cyclonic motion is generated. This confirms that the airflow is not merely rotational but turbulent in the relevant operating regions, supporting the use of a k–ε turbulence model.

3.2. Reduced-order model

The reduced-order model is introduced to replace repeated high-fidelity simulations during optimization. It is constructed from the reference solutions of the full multiphysics model and is valid within a prescribed domain of environmental and geometric inputs. This domain includes temperature, relative humidity, solar irradiance, wind conditions, and the main geometric variables of the tower, such as height, radius, wall thickness, and inlet configuration. The admissible domain is defined by the range of parameters used to generate the high-fidelity reference solutions.

The reduced representation is based on a Proper Orthogonal Decomposition (POD)-type modal framework applied to the relevant state variables:

$$\Phi(\mathbf{r}, t; \boldsymbol{\xi}) \approx \sum_{i=1}^{N} a_i(t, \boldsymbol{\xi}) \phi_i(\mathbf{r}), \tag{20}$$

where Φ represents the physical fields of interest, ϕ_i are dominant spatial modes, a_i are time- and parameter-dependent modal amplitudes, and $\boldsymbol{\xi}$ denotes the vector of environmental and geometric inputs. Each physical field (velocity, temperature, humidity, and mass flow rate) is represented through an expansion of this form.

The reduced model defines a continuous response surface between discrete high-fidelity simulations. In particular, solutions obtained for representative environmental conditions are projected onto the reduced-order space and interpolated to reconstruct a continuous annual response. This extended formulation allows transient and seasonal variability to be captured without repeatedly solving the full system of partial differential equations.

The main output of the reduced-order model is the harvested water volume,

$$V_{\text{water}} = f(\boldsymbol{\xi}), \tag{21}$$

which is subsequently used in the optimization stage. Since the reduced model is only valid within the parameter space used for its construction, the optimization is restricted to this admissible region.

The reduced-order model is coupled with an economic formulation of the tower geometry within the optimization framework, where the design is obtained by minimizing cost while maximizing annual water production. A detailed description of the snapshot generation, modal decomposition, and optimization procedure is provided in the Supplementary Material.

4. Environmental framework and construction of input variables

The performance of the cyclone condensation tower depends strongly on the local environmental conditions. For this reason, the numerical model is not defined only by geometric parameters, but also by a set of environmental inputs that describe the specific deployment context. In this work, the reference location corresponds to the Levante region of Spain, with Almeria considered as the primary case study because of its high solar irradiance, coastal humidity, agricultural water demand, and seasonal water stress.

The environmental framework includes ambient temperature, relative humidity, solar irradiance, wind velocity, and ground temperature. These variables define the boundary and forcing conditions used in the high-fidelity model and subsequently in the

reduced-order model. In particular, meteorological data from the ASHRAE-21 database, incorporated into COMSOL Multiphysics, are used to represent representative annual conditions for the Almeria station. These data provide the temporal evolution of temperature, humidity, solar radiation, and wind conditions required to simulate the tower response throughout the year.

Solar forcing is treated explicitly because it affects both the tower envelope and the auxiliary polyethylene tube used to heat water in the upper region of the structure. The spectral irradiance reaching the site is computed using SMARTS, together with solar-position data, and is used to determine the wavelength-dependent power received per unit area. The optical properties of the relevant materials, mainly clay-based wall material and polyethylene, are then considered to estimate how radiation is absorbed as a function of penetration depth. This is important because most of the absorbed solar energy remains confined near the exposed surface, while the thermal inertia of the wall limits heat penetration toward the internal condensation region.

To describe this attenuation, the supplementary model uses a wall-distance formulation together with a Beer–Lambert-type absorption law. This allows the absorbed radiation to be converted into an effective volumetric heat source inside the solid domains. The purpose of this calculation is not to impose an arbitrary wall temperature, but to determine whether external solar heating significantly perturbs the internal thermal regime. The results support the assumption that, for sufficiently thick walls, the condensation region is mainly governed by the cooled air entering through the underground ducts and therefore by the ground-temperature boundary condition, rather than by direct external heating.

Wind forcing is also included because the tower modifies the local flow field and because the external wind contributes to suction at the outlet through a Venturi-like effect. The wind velocity distribution around the structure is computed using a turbulence model, and an auxiliary ordinary differential equation is used to align the pressure drop and wind stress with the observed meteorological wind data. The resulting outlet velocity is then used to define the suction pressure acting at the top of the tower. This coupling between environmental wind, tower geometry, and outlet pressure is essential for representing the passive airflow that drives the system.

Overall, the environmental input construction links the deployment site, material properties, solar forcing, ground thermal stabilization, and wind–structure interaction into a consistent set of model inputs. Only the main assumptions are summarized here; the detailed derivation of the spectral irradiance model, optical absorption, wall-distance equation, ASHRAE data processing, wind-profile reconstruction, and Venturi pressure calculation is provided in the Supplementary Material.

5. Optimization framework

This section presents the optimization framework used to determine cost-efficient geometrical configurations of the cyclone condensation tower. The problem is formulated as a constrained optimization process in which the objective is to maximize annual water production while minimizing the economic cost associated with the tower geometry. Since repeated full high-fidelity simulations would be computationally prohibitive, the optimization is performed using the reduced-order model introduced in Section 3.2.

The proposed procedure can be understood as a meta-optimization strategy, since the optimization problem is itself preconditioned before the final search is performed. In a first stage, the geometric design space is restricted using symbolic and numerical calculations implemented in Mathematica. This preliminary step combines geometric and economic variables to identify admissible ranges for the tower dimensions, with particular attention to the wall thickness, which strongly affects material volume and cost. At the same time, the wall thickness cannot be reduced arbitrarily, since it must provide structural integrity and sufficient thermal inertia to stabilize the condensation region. In this sense, the geometric preconditioning does not only reduce cost, but also preserves the thermal relaxation time of the wall, so that the internal temperature field remains mainly governed by the underground intake ducts and soil temperature rather than by fast external thermal fluctuations.

In a second stage, the admissible geometries are evaluated through the high-fidelity COMSOL model for representative environmental conditions. The resulting reference solutions are used to construct a reduced-order model based on eigenvalues and eigenfunctions. These reduced solutions, obtained for selected representative days, are then interpolated to generate a temporally extended model capable of approximating the annual response. Finally, the interpolated reduced model is coupled through MATLAB/COMSOL LiveLink with a KKT-based constrained optimization, where the objective is to maximize harvested water while minimizing economic cost.

5.1. Reduced-order model for annual performance evaluation

A direct transient simulation of the complete finite-element model over a full year, with sub-daily time resolution, would be computationally unfeasible. This limitation becomes even more restrictive when atmospheric variability and changes in geometric design parameters must be included within an iterative optimization process. To overcome this difficulty, a reduced-order model is used to approximate the system response over the relevant environmental and geometric parameter space.

The reduced model is constructed from a set of high-fidelity numerical solutions, or *snapshots*, obtained for representative operating conditions. These snapshots describe the dynamic behavior of the main physical variables, including velocity, temperature, pressure, and relative humidity:

$$\mathbf{u}_{\text{out}}\left(\mathbf{r}_{\text{in,amb}}, t\right) = [\mathbf{u}_1, \mathbf{u}_2, \ldots, \mathbf{u}_n], \tag{22}$$

$$T_{\text{out}}\left(\mathbf{r}_{\text{in,amb}}, t\right) = [T_1, T_2, \ldots, T_n], \tag{23}$$

$$p_{\text{out}}\left(\mathbf{r}_{\text{in,amb}}, t\right) = [p_1, p_2, \ldots, p_n], \tag{24}$$

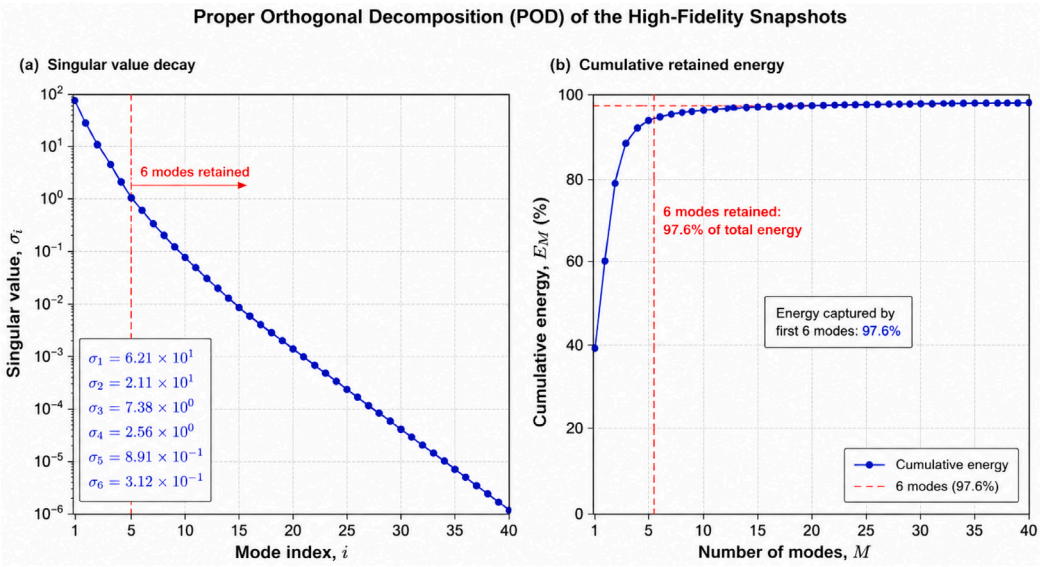


Fig. 5. POD analysis of the snapshot matrix obtained from the high-fidelity simulations. (a) Singular value decay on a logarithmic scale. (b) Cumulative retained energy as a function of the number of modes. The first six modes capture approximately 97.6% of the total modal energy and were therefore retained in the reduced-order model.

$$RH_{\text{out}}\left(\mathbf{r}_{\text{in,amb}}, t\right) = [RH_1, RH_2, \ldots, RH_n]. \tag{25}$$

From these snapshots, correlation matrices are built. For instance, for the velocity field,

$$\mathbf{C} = \frac{1}{n}\sum_{i=1}^{n} \mathbf{u}_i \mathbf{u}_i^T. \tag{26}$$

The associated eigenvalue problem is

$$\mathbf{C}\boldsymbol{\Phi} = \lambda\boldsymbol{\Phi}, \tag{27}$$

where the eigenvectors $\boldsymbol{\Phi}$ define the dominant spatial modes and the eigenvalues λ quantify the energetic relevance of each mode. Only the most significant modes are retained, thereby reducing the dimensionality of the system.

The number of retained modes was selected from the decay of the singular values associated with the snapshot correlation matrix. Fig. 5 shows that the dominant energetic content of the high-fidelity solutions is concentrated in the first modes. In particular, the first six modes capture approximately 97.6% of the cumulative modal energy. This threshold was adopted as a compromise between reconstruction accuracy and computational efficiency, allowing the reduced-order model to preserve the dominant coherent structures of the coupled thermo-fluid problem while keeping the optimization stage computationally tractable. It is important to emphasize that this reduced representation is used only within the interpolation domain defined by the high-fidelity training simulations. Therefore, the ROM is not employed as an extrapolatory surrogate outside the range of geometric and environmental parameters used to construct the snapshot set.

The physical fields are then projected onto the reduced basis. For example,

$$\mathbf{u}_{\text{out}}\left(\mathbf{r}_{\text{in,amb}}, t\right) \approx \sum_{i=1}^{m} a_i(t)\boldsymbol{\Phi}_i, \tag{28}$$

$$T_{\text{out}}\left(\mathbf{r}_{\text{in,amb}}, t\right) \approx \sum_{i=1}^{m} b_i(t)\boldsymbol{\Psi}_i, \tag{29}$$

where $a_i(t)$ and $b_i(t)$ are time-dependent modal coefficients. Instead of solving the full Navier–Stokes and heat-transfer equations at every time step, the reduced model evolves through the modal coefficients,

$$\frac{da_i(t)}{dt} = f_i(a_1, a_2, \ldots, a_m), \tag{30}$$

which drastically reduces the computational cost.

The model is extended to include both geometrical parameters and climatic inputs. The main geometric variables considered are the tower height H, wall thickness th, and base radius R_b. The environmental variables include ambient temperature, wind velocity, relative humidity, and solar forcing. High-fidelity simulations are performed for twelve representative days throughout

the year, including solstices, equinoxes, and intermediate dates selected to capture relevant seasonal changes in water production. These simulations define the interpolation domain of the reduced model and allow reconstruction of the annual behavior.

For the main variables involved in the optimization, the extended reduced model can be written as

$$\mathbf{u}(\mathbf{r}_{\text{probe}}, t; H, th, R_b) = \sum_{i=1}^{m} a_i(\mathbf{r}_{\text{in,amb}}, t; H, th, R_b)\Psi_i^{(u)}(H, th, R_b), \tag{31}$$

$$T(\mathbf{r}_{\text{probe}}, t; H, th, R_b) = \sum_{i=1}^{m} b_i(\mathbf{r}_{\text{in,amb}}, t; H, th, R_b)\Psi_i^{(T)}(H, th, R_b), \tag{32}$$

$$\dot{m}(\mathbf{r}_{\text{probe}}, t; H, th, R_b) = \sum_{i=1}^{m} c_i(\mathbf{r}_{\text{in,amb}}, t; H, th, R_b)\Psi_i^{(\dot{m})}(H, th, R_b), \tag{33}$$

$$RH(\mathbf{r}_{\text{probe}}, t; H, th, R_b) = \sum_{i=1}^{m} d_i(\mathbf{r}_{\text{in,amb}}, t; H, th, R_b)\Psi_i^{(RH)}(H, th, R_b). \tag{34}$$

The instantaneous harvested-water mass flow rate, $\dot{m}_{\text{water}}(t; H, th, R_b)$, is then integrated over time using the environmental data and the geometrical parameters defining each candidate design.

5.2. Objective function

The second key element of the optimization framework is the economic cost of the tower. The first approximation assumes that most construction and dismantling costs scale with the amount of material used. Under this assumption, the material volume V_m is computed from the difference between the outer and inner surfaces of revolution of the tower:

$$V_m = \pi \int_{z_b}^{z_t} \left[R_{\text{out}}^2(z) - R_{\text{in}}^2(z)\right] \, dz, \tag{35}$$

where $R_{\text{out}}(z)$ and $R_{\text{in}}(z)$ are the external and internal radius functions, respectively, and z_b and z_t define the vertical integration limits.

The internal radius is defined as

$$R_{\text{in}}(z) = \begin{cases} \cosh^{-1}\left(\dfrac{z + (H - z)\cosh(R_b)}{H}\right), & z_b \le z \le z_{\text{in}}, \\ R_t, & z_t \ge z > z_{\text{in}}, \end{cases} \tag{36}$$

with

$$z_{\text{in}} = \frac{H\left[\cosh(R_b) - \cosh(R_t)\right]}{\cosh(R_b) - 1}. \tag{37}$$

The external radius is

$$R_{\text{out}}(z) = \begin{cases} \cosh^{-1}\left(\dfrac{z + (H + th - z)\cosh(R_b + th)}{H + th}\right), & z_0 \le z \le z_{\text{out}}, \\ R_t + th, & z_{\text{out}} < z \le z_t, \end{cases} \tag{38}$$

where

$$z_{\text{out}} = \frac{(H + th)\left[\cosh(R_b + th) - \cosh(R_t + th)\right]}{\cosh(R_b + th) - 1}. \tag{39}$$

The sensitivity of V_m with respect to the geometric variables shows that wall thickness has the strongest influence on total material volume. This occurs because increasing th modifies the outer surface over the full height of the structure, amplifying its contribution relative to height or base radius alone. Consequently, wall thickness becomes the first geometric variable to be constrained in the optimization process. As shown in Fig. 6, wall thickness remains a dominant cost-driving parameter regardless of the assumed cost scenario. Even when all construction components are assigned identical unit costs, the thickness has a decisive effect on the final cost. If the foundation is assumed to be constructed from reinforced concrete, with a cost significantly higher than the remaining tower components, this dominance becomes even more pronounced.

However, material volume alone does not fully describe construction cost. The total cost also depends on how material is extracted, moved, lifted, and assembled. For this reason, the tower height is further decomposed into two contributions: a buried section H_{room} and an exposed section H_{top}. The buried section accounts for excavation work, whereas the exposed section accounts for the gravitational work required to lift material above ground level. This distinction allows the cost model to include not only the amount of matter used, but also the energetic effort required to place/remove it.

The total cost is therefore decomposed as

$$\begin{aligned} C_{\text{total}}(V_m) =& C_{\text{trans}}(V_m) + C_{\text{reso}}(V_m) + C_{\text{labor}}(V_m) + C_{\text{adi}}(V_m) \\ &+ C_{\text{dis}}(V_m), \end{aligned} \tag{40}$$

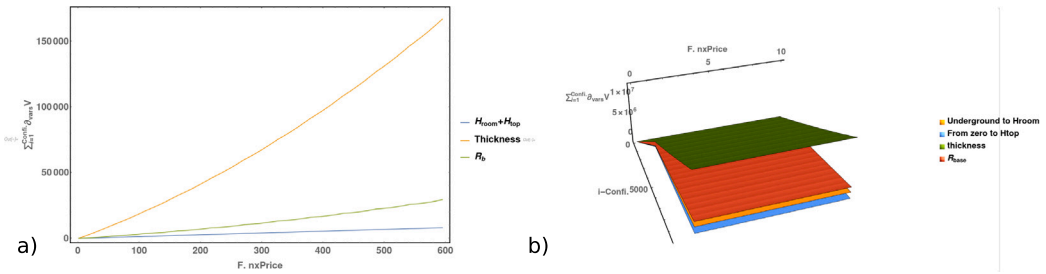


Fig. 6. Influence of wall thickness on total cost under two scenarios. (a) When the foundation is assumed to be made of reinforced concrete, with a cost up to ten times higher than the remaining tower components, wall thickness remains a dominant factor in the final cost. (b) Even when all construction elements are assumed to have identical unit costs, wall thickness continues to exert a decisive influence on the total cost of the tower.

where C_{trans} denotes transportation cost, C_{reso} material or resource cost, C_{labor} labor cost, C_{adi} additional construction costs, and C_{dis} dismantling cost.

In the refined cost model, three energetic contributions are added to the material-volume estimate: excavation of the buried chamber, controlled mainly by H_{room} and R_{room}, excavation of the intake-pipe trenches, controlled by the pipe length L_{pipe} and trench depth d_{trench}, gravitational lifting of wall material, controlled mainly by H_{top}, th, and R_{room}.

These contributions are particularly relevant when the system is intended for low-technology or low-machinery construction scenarios. If a finite workforce is assumed, the mechanical work associated with excavation and lifting cannot be delivered instantaneously. Instead, total work is converted into construction time, and construction time into labor cost. Thus,

$$C_{\text{labor}} \propto T_{\text{construction}}, \tag{41}$$

so economic cost and construction time are controlled by the same physical constraint: the limited rate at which work can be supplied.

To quantify the influence of each geometric and constructive variable on the total cost, we define the normalized sensitivity

$$S_x = \left| \frac{x}{C} \frac{\partial C}{\partial x} \right|, \tag{42}$$

where C may denote either the total economic cost or the construction time, and

$$x \in \left\{ H_{\text{room}}, H_{\text{top}}, th, R_{\text{room}}, L_{\text{pipe}}, d_{\text{trench}} \right\}. \tag{43}$$

Since the cost function contains numerical integrations and piecewise-defined geometric functions, the derivatives are evaluated numerically using finite differences. A cumulative global sensitivity is then computed over the sampled design space:

$$S_x^{\text{cum}} = \sum_{i=1}^{N} S_x^{(i)}. \tag{44}$$

This quantity provides a global measure of the influence of each variable over the explored configurations rather than a local derivative at a single design point.

The global sensitivity analysis shows that the same variables dominate both economic cost and construction time. Wall thickness remains the principal cost driver because it controls material volume and therefore also lifting work. The exposed height H_{top} becomes increasingly important once gravitational lifting is included, while H_{room} and d_{trench} become relevant when excavation dominates. The pipe length L_{pipe} contributes approximately linearly through trench excavation, but remains secondary unless the intake network becomes excessively long.

A key outcome is that the ranking of variables obtained from the economic-cost sensitivity is nearly identical to the ranking obtained from construction-time sensitivity. This is expected because labor cost is proportional to construction time, and construction time is determined by the total mechanical work required. Therefore, minimizing economic cost also tends to minimize execution time.

This result allows the definition of a feasible design domain before solving the full water-production optimization problem. The variables are bounded as

$$H_{\text{room}} \in [H_{\text{room}}^{\min}, H_{\text{room}}^{\max}], \quad H_{\text{top}} \in [H_{\text{top}}^{\min}, H_{\text{top}}^{\max}], \quad th \in [th^{\min}, th^{\max}],$$

$$R_{\text{room}} \in [R_{\text{room}}^{\min}, R_{\text{room}}^{\max}], \quad L_{\text{pipe}} \in [L_{\text{pipe}}^{\min}, L_{\text{pipe}}^{\max}], \quad d_{\text{trench}} \in [d_{\text{trench}}^{\min}, d_{\text{trench}}^{\max}].$$

The sensitivity results further reduce this space through the following cost-minimizing trends $th \to th^{\min}$, $H_{\text{top}} \lesssim \alpha H_{\text{room}}$, $H_{\text{room}} \leq H_{\text{room}}^{*}$, $L_{\text{pipe}} \to L_{\text{pipe}}^{\min}$, $d_{\text{trench}} \approx d_{\text{trench}}^{\min}$. These inequalities do not define the final optimum by themselves. Instead, they define a reduced feasible design envelope in which the subsequent optimization of water production is performed. The feasible domain is illustrated in Fig. 7. The diagram can be interpreted as a phase map of the construction process: one region is dominated by

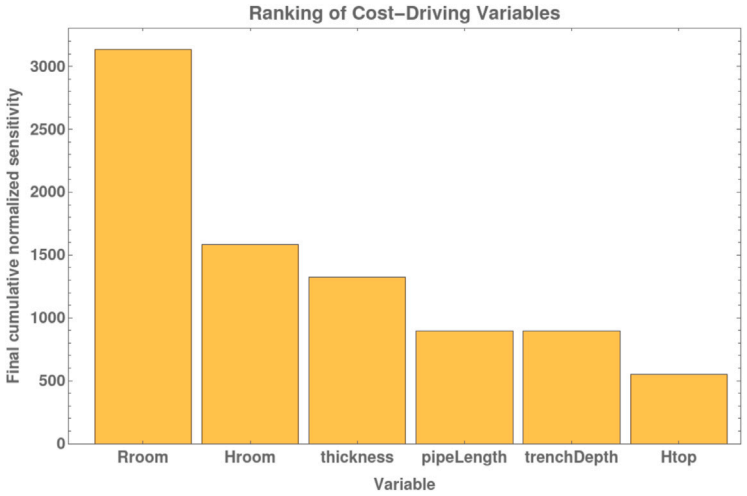


Fig. 7. Feasible geometric design domain derived from the global sensitivity analysis. The shaded region represents configurations satisfying the cost-minimizing inequalities obtained for wall thickness, excavation depth, and exposed height. The boundary separates excavation-dominated and lifting-dominated cost regimes.

excavation cost, mainly associated with increasing H_{room}, while the other is dominated by lifting cost, associated with increasing H_{top}. The transition between these regimes defines a practical trade-off between buried and exposed height. In addition, the admissible domain narrows as wall thickness increases, reinforcing the conclusion that th must be minimized within structural and thermal constraints.

Once this feasible geometric domain has been established, the optimization objective is formulated as the minimization of the cost per unit of water production:

$$\min_{\mathbf{x}} FO(\mathbf{x}) = \frac{C_{\text{eco}}(\mathbf{x})}{\frac{V_{\text{water}}(\mathbf{x})}{T}} = \frac{C_{\text{total}}(V_m)}{\frac{1}{T}\int_0^T \dot{m}_{\text{water}}(t; H, th, R_b)\, dt}. \tag{45}$$

The design vector is defined as

$$\mathbf{x} = (H, th, R_b, \theta_1, \Delta_1, \theta_2, \Delta_2). \tag{46}$$

The parameters θ_1, Δ_1, θ_2, and Δ_2 describe the internal conical trapping profiles. Specifically, θ_1 and θ_2 are the angles formed by the lower and upper conical panels with respect to the vertical axis, while Δ_1 and Δ_2 are their corresponding generatrix lengths. These parameters affect the internal flow structure, residence time, and condensation efficiency, and are therefore included in the optimization even though they are not part of the external tower envelope.

Because the economic cost is strongly related to the geometric and energetic cost of construction, the objective can also be expressed in simplified form as

$$\min_{\mathbf{x}} FO(\mathbf{x}) = \frac{V_m(H, th, R_b, \theta_1, \Delta_1, \theta_2, \Delta_2)}{\langle V \rangle_{\text{H}_2\text{O}}(H, th, R_b, \theta_1, \Delta_1, \theta_2, \Delta_2)}, \tag{47}$$

where $\langle V \rangle_{\text{H}_2\text{O}}$ is the average harvested water volume over the considered period. This expression represents the material-equivalent cost per unit of collected water and is the quantity minimized in the optimization process (see Fig. 8).

The complete optimization workflow is summarized in Fig. 8. The extended reduced-order model is coupled to MATLAB through COMSOL LiveLink, allowing the geometrical design variables to be iteratively modified and the corresponding water production to be evaluated within the previously defined feasible domain. This procedure enables the optimization to be performed with substantially lower computational cost than would be required by repeated evaluations of the full multiphysics model.

5.3. Constraints and KKT formulation

In the KKT optimization, the total tower height is written as $H = H_{\text{room}} + H_{\text{top}}$. The variables H_{room}, H_{top}, L_{pipe}, and d_{trench} are used in the preliminary cost-sensitivity analysis to restrict the admissible geometric domain, while the final optimization is performed on the reduced design vector $\mathbf{x}$.

The design variables are subject to feasibility constraints based on constructive, geometric, and physical considerations:

$$10\,\text{m} \le H \le 24\,\text{m}, \qquad 0.35\,\text{m} \le th \le 1.2\,\text{m}, \qquad 2\,\text{m} \le R_b \le 4\,\text{m},$$
$$3\,\text{m} \le \Delta_1 \le 7\,\text{m}, \qquad 1.5\,\text{m} \le \Delta_2 \le 3\,\text{m},$$

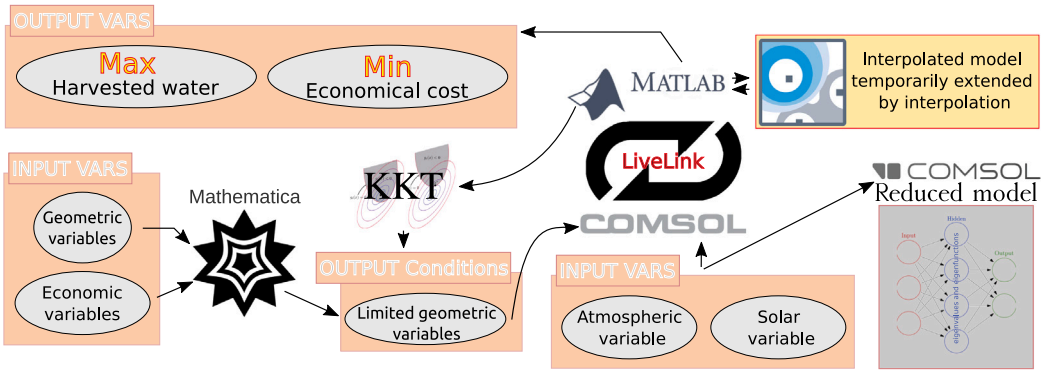


Fig. 8. Optimization workflow implemented through MATLAB LiveLink with COMSOL. The extended reduced-order model is used to evaluate system performance while varying the geometrical parameters of the tower. This approach enables geometry optimization aimed at maximizing water production while significantly reducing simulation time.

$$\frac{\pi}{13} \le \theta_1 \le \frac{\pi}{3}, \qquad \frac{\pi}{13} \le \theta_2 \le \frac{\pi}{4}.$$

These constraints are written as inequality functions $g_i(\mathbf{x}) \le 0$:

$$g_1(\mathbf{x}) = 10 - H \le 0, \quad g_2(\mathbf{x}) = H - 24 \le 0, \quad g_3(\mathbf{x}) = 0.35 - th \le 0,$$
$$g_4(\mathbf{x}) = th - 1.2 \le 0, \quad g_5(\mathbf{x}) = 2 - R_b \le 0, \quad g_6(\mathbf{x}) = R_b - 4 \le 0,$$
$$g_7(\mathbf{x}) = 3 - \Delta_1 \le 0, \quad g_8(\mathbf{x}) = \Delta_1 - 7 \le 0, \quad g_9(\mathbf{x}) = 1.5 - \Delta_2 \le 0,$$
$$g_{10}(\mathbf{x}) = \Delta_2 - 3 \le 0, \quad g_{11}(\mathbf{x}) = \frac{\pi}{13} - \theta_1 \le 0, \quad g_{12}(\mathbf{x}) = \theta_1 - \frac{\pi}{3} \le 0,$$
$$g_{13}(\mathbf{x}) = \frac{\pi}{13} - \theta_2 \le 0, \quad g_{14}(\mathbf{x}) = \theta_2 - \frac{\pi}{4} \le 0.$$

The constrained optimization problem is solved using the Karush–Kuhn–Tucker conditions [13,14]. The Lagrangian is

$$\mathcal{L}(\mathbf{x}, \lambda) = FO(\mathbf{x}) + \sum_{i=1}^{14} \lambda_i g_i(\mathbf{x}), \tag{48}$$

where λ_i are the Lagrange multipliers. The KKT conditions are:

1. **Primal feasibility:** $g_i(\mathbf{x}) \le 0, \quad i = 1, \dots, 14.$
2. **Stationarity:** $\nabla_{\mathbf{x}} \mathcal{L}(\mathbf{x}, \lambda) = \nabla FO(\mathbf{x}) + \sum_{i=1}^{14} \lambda_i \nabla g_i(\mathbf{x}) = 0.$
3. **Dual feasibility:** $\lambda_i \ge 0, \quad i = 1, \dots, 14.$
4. **Complementary slackness:** $\lambda_i g_i(\mathbf{x}) = 0, \quad i = 1, \dots, 14.$

These conditions ensure that the optimal design satisfies the feasible ranges of all geometric variables while minimizing the cost-to-water-production ratio.

5.4. Role of wall thickness in the optimization

A sensitivity analysis shows that wall thickness has a dominant effect on the total material volume and therefore on economic cost. This is expected because increasing the wall thickness modifies the volume over the full height of the tower and affects both the external and internal radii. To account for this effect, the objective function can include a weighting factor associated with th:

$$FO(\mathbf{x}) = \frac{w_{th}\, th\, V_m(H, th, R_b, \theta_1, \Delta_1, \theta_2, \Delta_2)}{\langle V \rangle_{\mathrm{H_2O}}(H, th, R_b, \theta_1, \Delta_1, \theta_2, \Delta_2)}, \tag{49}$$

where w_{th} emphasizes the influence of wall thickness on the cost function.

This weighting can also be interpreted within the KKT framework by assigning higher sensitivity to the constraints associated with th, namely g_3 and g_4. In practice, this reflects the fact that wall thickness has a stronger influence on material consumption than the other primary geometric parameters.

5.5. Generalized eigenvalue interpretation

To solve the constrained optimization problem efficiently, the stationarity condition of the KKT system can be interpreted through a generalized eigenvalue formulation. If the objective function and active constraints are approximated locally by quadratic or

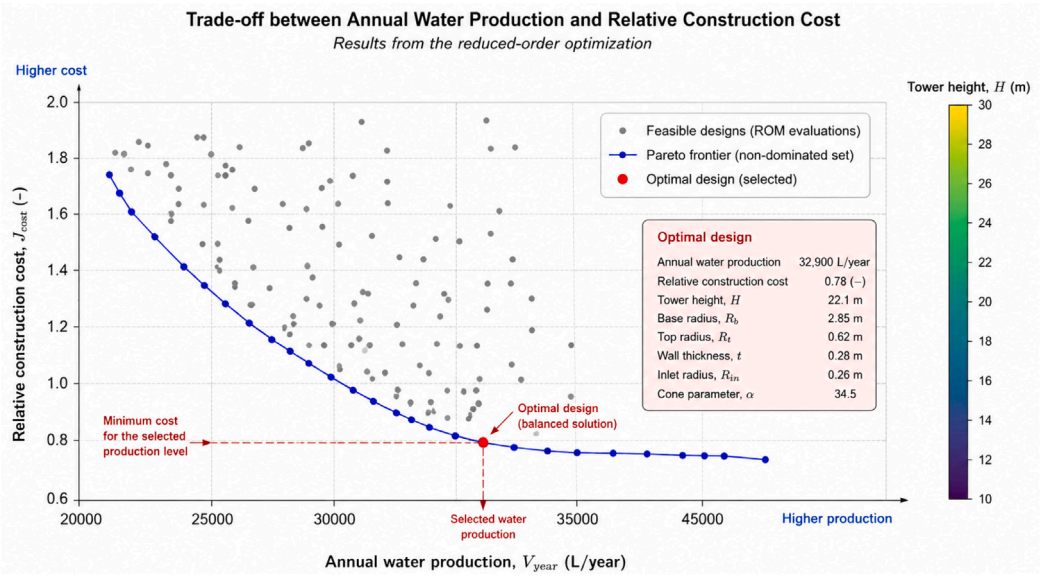


Fig. 9. Trade-off between annual water production and relative construction cost for the feasible geometrical configurations explored during the optimization process. Gray points represent admissible configurations evaluated through the reduced-order model, the blue curve indicates the Pareto-like frontier, and the red point corresponds to the selected optimal design.

bilinear forms, the gradients appearing in the stationarity condition become linear in $\mathbf{x}$. The system can then be expressed as

$$\mathbf{A}\mathbf{x} = \lambda \mathbf{B}\mathbf{x}, \tag{50}$$

where $\mathbf{A}$ represents the contributions associated with the Hessian of the Lagrangian, while $\mathbf{B}$ contains the gradients of the active constraints. This generalized eigenvalue formulation provides an analytical framework for identifying optimal parameter directions while balancing the objective function and constraints.

In the implementation, COMSOL LiveLink for MATLAB is used to evaluate the reduced-order model and update the matrices involved in the optimization process. This makes it possible to automate the iterative adjustment of the design variables and enforce feasibility constraints while maintaining a low computational cost.

To further analyze the optimization framework, Fig. 11 presents the trade-off between annual water production and relative construction cost obtained from the reduced-order optimization procedure. Each point corresponds to a feasible geometrical configuration evaluated within the admissible parameter space.

The results reveal the existence of a Pareto-like frontier separating inefficient configurations from near-optimal solutions. Increasing water production generally requires larger geometrical dimensions and therefore higher construction cost. However, beyond a certain threshold, the marginal gain in harvested water becomes progressively smaller relative to the additional material and energetic cost required for construction.

The selected optimal configuration corresponds to the region where the balance between annual water production and construction cost is most favorable, according to the objective function defined in Eq. (45).

6. Results

6.1. Computational strategy and reduced-domain simulations

The high-fidelity simulations were organized to reduce computational cost while preserving the relevant multiphysics couplings. First, a steady-state simulation was performed to obtain a physically consistent initial condition for the transient calculations. This step is important because the full transient problem couples turbulent airflow, heat transfer in solids and fluids, moisture transport, and phase change. Starting the transient computation from a converged steady-state solution improves numerical convergence and reduces the computational time required for each daily simulation.

To further reduce the computational burden, the geometry was exploited through symmetry and only one quarter of the tower was simulated in the transient calculations. The fluid region, corresponding to the moist air inside the tower, and the solid region, corresponding to the tower wall, were treated as separate domains in a COMSOL assembly rather than as a single union. The thermodynamic exchange between both domains was imposed through boundary-pair conditions at the fluid–solid interface. This approach allows the fluid and solid physics to be solved in their respective domains while preserving thermal coupling across the internal wall.

The simulation workflow therefore consists of four stages. First, a steady-state calculation is obtained for each geometrical configuration. Second, the steady-state solution is used as the initial condition for a one-day transient simulation. Third, the resulting fields are processed through an eigenvalue–eigenfunction analysis to construct the reduced-order model. Finally, the reduced model is used to evaluate annual performance and to support the optimization process.

6.2. Relative humidity field and condensation criterion

It should be emphasized that the purpose of the present section is to validate the consistency between the high-fidelity model, the reduced-order model, and the compact Gaussian approximation, rather than to evaluate the optimal tower configuration obtained in the optimization stage. Consequently, the results reported in Table 1 and Fig. 11 correspond to a representative tower geometry selected within the admissible design space, whose performance is close to the optimum but not identical to the final optimal solution identified in Section 5. The optimal configuration is discussed separately through the multi-objective optimization results presented in Fig. 9, whereas the present section focuses exclusively on assessing the predictive capability of the proposed reduced-order methodology.

The local water harvesting mechanism is controlled by the relative humidity field inside the tower. Condensation is assumed to occur in regions where the local relative humidity exceeds saturation, i.e. where $RH \geq 1$. Fig. 10 shows the relative humidity distribution and the location of the surface probe used to evaluate the temporal evolution of saturation near the lower part of the tower. The figure also shows that, for several representative days, the relative humidity exceeds the saturation threshold during extended periods, particularly in summer months. The harvested water is computed from the excess vapor transported through the collection section. A water harvesting indicator is introduced as

$$WHI_{RH}(\mathbf{r},t) = \begin{cases} 1, & RH(\mathbf{r},t) \geq 1, \\ 0, & RH(\mathbf{r},t) < 1. \end{cases} \tag{51}$$

The instantaneous condensed-water mass flow rate is then calculated as

$$\dot{m}_{\mathrm{H_2O}}(t) = \iint_S \left(\rho(\mathbf{r},t) q_w^{\mathrm{exc}}(\mathbf{r},t)\right) \mathbf{u}(\mathbf{r},t) \cdot d\mathbf{S}, \tag{52}$$

where ρ is the moist-air density, q_w^{exc} is the excess water-vapor mass fraction available for condensation, $\mathbf{u}$ is the velocity field, and S is the collection section. The corresponding daily harvested volume is

$$V_{\mathrm{H_2O,day}} = \frac{1}{\rho_{\mathrm{H_2O}}} \int_0^{24\ h} \left[\iint_S \left(\rho q_w^{\mathrm{exc}}\right) \mathbf{u} \cdot d\mathbf{S} \right] dt. \tag{53}$$

This formulation filters out non-saturated regions and accounts only for the fraction of water vapor that can condense and be collected.

6.3. Daily and annual water production

Table 1 compares the harvested water predicted by the high-fidelity model, the extended reduced-order model, and the compact Gaussian model for representative days throughout the year. The results show a strong seasonal dependence. Winter and early spring conditions produce little or no water, while the highest yields occur in summer, with a maximum daily production close to 145 L in mid-August. The reduced-order model predicts an annual production of approximately 20943 L, corresponding to an average of about 57 L/day. A compact Gaussian model provides a very similar annual estimate, 20895 L, also corresponding to an average of approximately 57 L/day. This agreement supports the use of the compact model as a fast surrogate for annual performance estimation.

The Gaussian model is written as

$$V_{\mathrm{day}}^{\mathrm{Gauss}}(d_n) = V_0 \exp\left[-\frac{\left((d_n - \mu)^2\right)^{27/20}}{2\sigma^2} \right], \tag{54}$$

with $V_0 = 142$ L, $\mu = 230$, and $\sigma = 275$. Fig. 11 compares the high-fidelity daily values, the extended reduced-order response, and the Gaussian compact model. The three descriptions show consistent seasonal behavior, with negligible production in winter and maximum production during summer.

These results show that the tower is strongly seasonal under the selected environmental conditions. The highest production occurs when warm temperatures, high humidity, and sufficient solar forcing combine to maintain the internal flow and condensation process. Conversely, winter conditions remain below the saturation threshold for most of the day, limiting water production regardless of geometrical optimization.

Additional numerical results, including the complete description of the computational domains, boundary conditions, mesh implementation, wind-loading analysis, velocity and temperature fields, and extended transient simulations, are provided in the Supplementary Material.

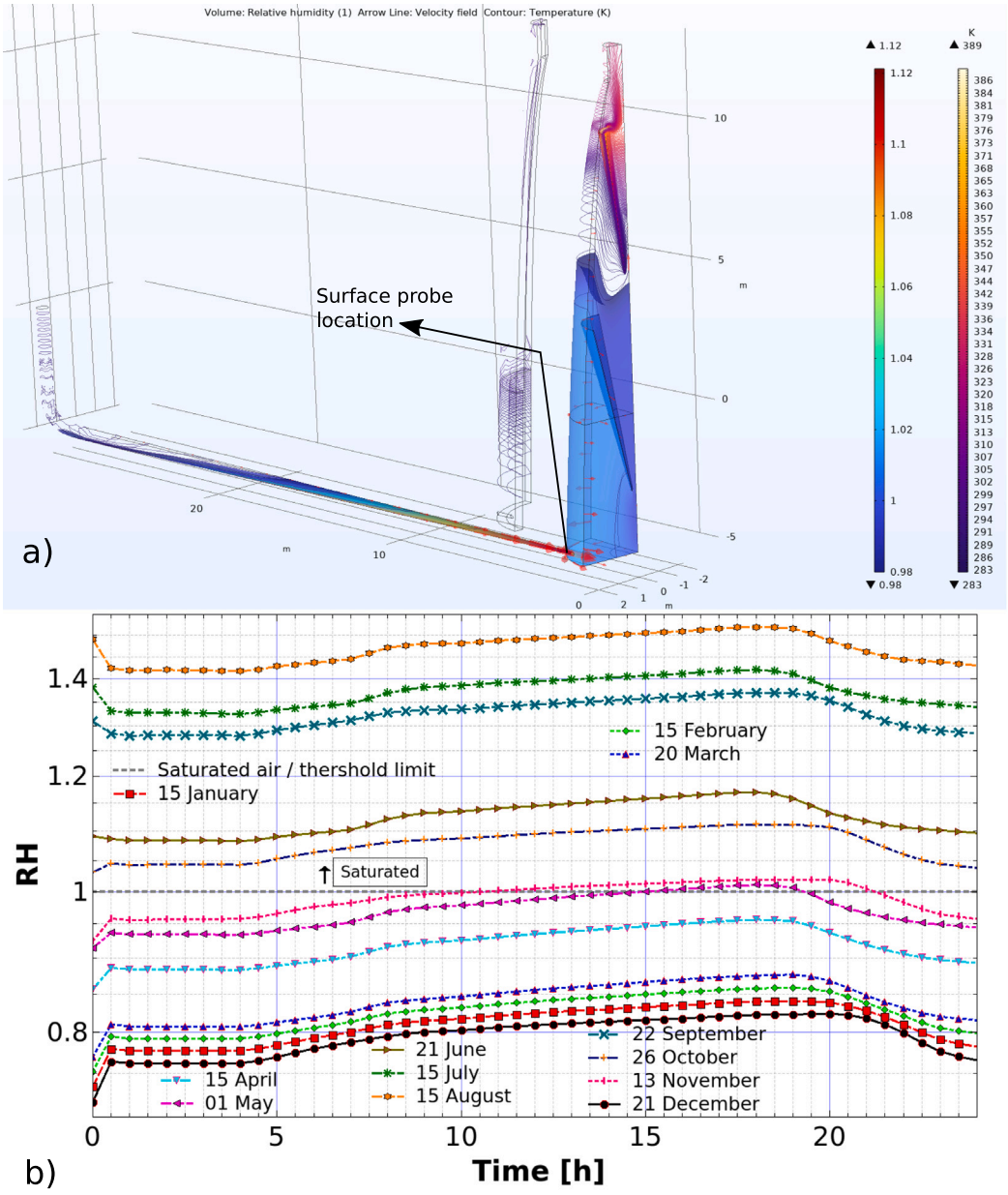


Fig. 10. Relative humidity field and temporal evolution at the surface probe. (a) Relative humidity distribution inside the tower, together with velocity-field arrows and temperature contours. The probe is located near the lower condensation region, close to the tangential intake. (b) Relative humidity evolution for representative days throughout the year. The saturation threshold $RH = 1$ separates non-condensing and condensing regimes. Summer conditions show sustained supersaturation, while winter conditions remain below the condensation threshold.

7. Conclusions

This work presents a unified framework for the design and optimization of a cyclone condensation tower for atmospheric water harvesting. The proposed system combines passive thermodynamic, fluid-dynamic, and geometric mechanisms to induce continuous airflow, cooling, and condensation without the need for external mechanical energy input.

A high-fidelity multiphysics model was developed to describe the coupled behavior of turbulent airflow, heat transfer, and moisture transport. To enable large-scale design exploration, a reduced-order model was constructed, allowing efficient evaluation of annual performance under realistic environmental conditions. The agreement between the full model, the reduced-order formulation, and a compact Gaussian approximation demonstrates the robustness of the proposed modeling strategy.

Table 1
Daily harvested water for representative dates and estimated annual production. The full model provides discrete reference values, while the reduced-order and Gaussian models reconstruct the annual response.

Date	Full model	Reduced model	Gaussian model
January 15	0	0	2.85 ml
February 15	0	0	25.7 ml
March 20	0	0	1 l
April 15	0	1.3 ml	7 l
May 1	22 l	20.4 l	17.5 l
June 21	97 l	98.9 l	97 l
July 15	131 l	128.5 l	130 l
August 15	144 l	144.8 l	142 l
September 22	121 l	124.5 l	129 l
October 26	88 l	77.6 l	77 l
November 13	40 l	48.7 l	6.8 l
December 21	0	0	3.39 l
Annual total	–	**20943 l**	**20895 l**

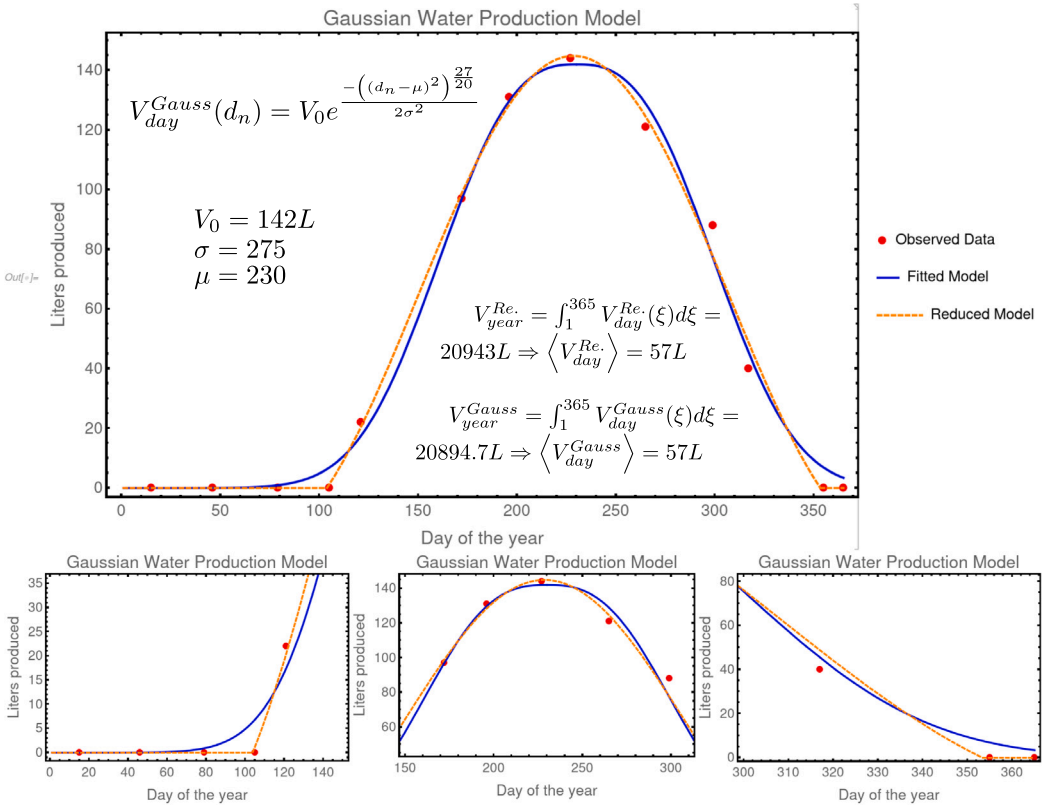


Fig. 11. Annual water production predicted by the full model, the extended reduced-order model, and the Gaussian compact model. The red points correspond to high-fidelity simulations for representative days, the dashed curve represents the reduced-order model, and the solid curve corresponds to the Gaussian fit. The reduced model predicts an annual production of 20943 L, while the Gaussian model gives 20894.7 L, both corresponding to an average daily production of approximately 57 L.

A key contribution of this work is the introduction of an energy-based cost formulation, in which economic cost and construction time are directly linked through the mechanical work required for excavation, material handling, and lifting. This approach reveals that cost and time are governed by the same physical constraint, namely the limited rate at which work can be supplied. As a consequence, optimizing the system with respect to economic cost inherently leads to near-optimal construction times.

The global sensitivity analysis identifies wall thickness as the dominant design parameter, followed by the exposed height of the tower, which strongly influences gravitational lifting work. Excavation-related variables become relevant only in configurations with large underground components, while the intake-pipe network contributes primarily as a secondary linear effect. These results allow the definition of a reduced feasible design domain prior to the full optimization of water production.

The optimization framework combines this preconditioned design space with a constrained formulation based on Karush–Kuhn–Tucker conditions. This strategy enables the identification of geometries that balance material usage, construction effort, and water production efficiency.

Under the environmental conditions considered for the Almeria region, the system exhibits strong seasonal behavior, with peak water production occurring during summer months. Annual production estimates obtained from the reduced-order model are consistent with both high-fidelity simulations and compact analytical approximations.

Overall, the results demonstrate that the design of atmospheric water-harvesting systems cannot be addressed solely as a geometric or fluid-dynamic problem, but must incorporate construction energetics and environmental coupling. The methodology presented here provides a scalable framework for optimizing such systems in resource-constrained environments, and can be extended to other passive infrastructure technologies where energy, time, and cost are intrinsically coupled.

Future work will focus on extending the environmental analysis to additional climatic regions, refining the structural and material models, and integrating the system within distributed water and energy infrastructures.

CRediT authorship contribution statement

P. González-Rodelas: Writing – review & editing, Supervision, Methodology, Validation. **G. Klochok:** Software, Formal analysis, Investigation. **E. Moreno:** Writing – original draft, Software, Methodology, Formal analysis, Conceptualization.

Acknowledgments

The last author would like to express his gratitude to Juan de Dios Wilhelmi, whose undergraduate thesis work provided the inspiration and conceptual foundations for the development of this work.

Appendix A. Supplementary data

Supplementary material related to this article can be found online at https://doi.org/10.1016/j.matcom.2026.07.037.

References

[1] Hannah Ritchie, Max Roser, Water use and stress, Our World Data (2018) https://ourworldindata.org/water-use-stress.
[2] Antonio Valero Capilla, Alicia Valero Delgado, Thanatia: The Destiny of the Earth's Mineral Resources, World Scientific, 2014.
[3] Alicia Valero, Antonio Valero, Guiomar Calvo, The Material Limits of Energy Transition: Thanatia, Springer Cham, 2021, https://doi.org/10.1007/978-3-030-78533-8.
[4] Zahra Ahrestani, Sadegh Sadeghzadeh, Hosein Banna Motejadded Emrooz, An overview of atmospheric water harvesting methods, the inevitable path of the future in water supply, RSC Adv. 13 (2023) 10273–10307.
[5] W. Haaf, K. Friedrich, G. Mayr, J. Schlaich, Solar chimneys part I: Principle and construction of the pilot plant in manzanares, Int. J. Sol. Energy (1983).
[6] Cristiana B. Maia, Felipe V.M. Silva, Vinícius L.C. Oliveira, Lawrence L. Kazmerski, An overview of the use of solar chimneys for desalination, Sol. Energy 183 (2019) 83–95.
[7] B.A. Kashiwa, Corey B. Kashiwa, The solar cyclone: A solar chimney for harvesting atmospheric water, Energy 33 (2) (2008) 331–339, 19th International Conference on Efficiency, Cost, Optimization, Simulation and Environmental Impact of Energy Systems.
[8] Alexander Bolonkin, Production of freshwater and energy from earth's atmosphere, Smart Grid Renew. Energy (2011).
[9] Tingzhen Ming, Tingrui Gong, Renaud K. de Richter, Wei Liu, Atit Koonsrisuk, Freshwater generation from a solar chimney power plant, Energy Convers. Manage. 113 (2016) 189–200.
[10] Qichao Hu, Xiaoxin Wang, Ahmed Gamil, Peiwen Li, Experimental study of desalination using a system integrated by a glass-covered solar collection water basin and a heat dissipating chimney, Energy Nexus 9 (2023) 100171.
[11] Air Water FZCO, Atmospheric water generator plant , 2023,.
[12] COMSOL, Inc., COMSOL Multiphysics (Version 6.2), COMSOL, Inc., Burlington, Massachusetts, 2024.
[13] M.A. Bhatti, Practical Optimization Methods: With Mathematica® Applications, Springer New York, 2012.
[14] A. Antoniou, W.S. Lu, Practical Optimization: Algorithms and Engineering Applications, Springer US, 2007.